ERK signaling dissolves ERF repression condensates in living embryos

Claire J. Weaver[a,b], Aleena L. Patel[a,b,1], Stanislav Y. Shvartsman[a,b,c], Michael S. Levine[a,b,2], and Nicholas Treen[a,2]

[a]Lewis-Sigler Institute for Integrative Genomics, Princeton University, Princeton, NJ 08544; [b]Department of Molecular Biology, Princeton University, Princeton, NJ 08544; and [c]Flatiron Institute, Simons Foundation, New York, NY 10010

Contributed by Michael S. Levine; received November 9, 2021; accepted January 7, 2022; reviewed by Shigeki Fujiwara and Alberto Stolfi

Phase separation underlies the organization of the nucleus, including the biogenesis of nucleoli and the packaging of heterochromatin. Here we explore the regulation of transcription factor condensates involved in gene repression by ERK signaling in gastrulating embryos of a simple proto-vertebrate (*Ciona*). ERK signaling induces nuclear export of the transcriptional repressor Ets-2 repressive factor (ERF), which has been linked to various human developmental disorders. Using high-resolution imaging, we show that ERF is localized within discrete nuclear condensates that dissolve upon ERK activation. Interestingly, we observe dynamic pulses of assembly and dissociation during interphase, providing visualization of a nuclear phase separation process regulated by cell signaling. We discuss the implications of these observations for producing sharp on/off switches in gene activity and suppressing noise in cell–cell signaling events.

developmental biology | transcriptional repression | phase separation

Liquid–liquid phase separation (LLPS) has emerged as a major mechanism for cellular organization (1), including the biogenesis of nucleoli and other components of the nucleus (2, 3). Within nuclei, LLPS has also been implicated in the assembly of the RNA polymerase II preinitiation complex at poised promoters (4–6), as well in transcriptional silencing. HP1 chromocenters display liquid behavior (7, 8), and the transcriptional repressor Hes.a was recently shown to possess liquid properties when associated with the Groucho (Gro/TLE) corepressor (9). Hes.a condensates formed when the sequence-specific DNA-binding domain of Hes.a and the C-terminal WRPW motif were both present. Condensates were lost upon removal of the WRPW motif, resulting in uniform distribution of Hes.a throughout the nucleus. By contrast, mutations in the basic helix–loop–helix (bHLH) DNA-binding domain resulted in the formation of larger condensates due to more frequent fusion events, evocative of liquid droplets (9). Hes.a/Gro condensates are stable throughout interphase when expressed in living *Ciona* embryos, finally dissolving at the onset of mitosis (9). These observations point toward a simple mechanism for transcriptional repression, whereby Hes.a/Gro condensates exclude transcriptional activators at silent loci (9).

Transcriptional repressors are often deployed to silence gene expression in the absence of cell signaling (10). This default repression is inhibited upon cell signaling to activate gene expression (10, 11). Here, we explore the possibility that cell signaling derepresses gene silencing by influencing the assembly and disassembly of repression condensates. In ERK signaling, the activation of a receptor by its ligand (e.g., fibroblast growth factor/FGF) triggers a phosphorylation cascade that culminates in the activation and nuclear translocation of ERK (12). Previous studies suggest ERK signaling antagonizes transcriptional repressors such as Capicua, Yan, and ERF (13–16), in addition to inducing the activities of transcriptional activators such as ETS and Pointed (17).

In the *Ciona* embryo, FGF/ERK signaling is pervasively used to specify a variety of cell types, including cardiomyocytes and neuronal cell types in the central nervous system (18–20). This signaling acts upon ETS-class transcription factors—typically interpreted as activators, although derepression mechanisms are likely to participate as well. The maternally expressed *Ciona* ortholog of the human Ets-2 repressive factor (ERF) is a strong candidate for one such repressor as it persists throughout early development (21). Mammalian ERF is a sequence-specific repressor that recognizes canonical ETS binding sites (15, 22, 23) and is exported from the nucleus upon ERK activation (15, 23). It has been implicated in a variety of human diseases, including craniofacial disorders (24).

We present evidence that ERF forms spherical condensates during *Ciona* embryonic development and FGF/ERK signaling leads to their dissolution and export from the nucleus. There is a tight correlation between the formation of ERF condensates, association with the Gro corepressor, and transcriptional silencing of FGF/ERK target genes. Unexpectedly, ERF condensates exhibit a pulse of dissolution and reformation during interphase, suggesting transient rather than sustained FGF/ERK signaling. We suggest that regulating the assembly and disassembly of ERF condensates suppresses noise and produces sharp, switch-like induction of gene expression.

Results

A survey of the *Ciona* genome identified two putative orthologs of the human ERF repressor. One is maternally expressed in

Significance

Transcriptional repression is essential for correct gene expression, and failure to repress genes appropriately is associated with many diseases. Recently, evidence is accumulating that phase separation is an important component of transcriptional repression. We show that the extracellular signal-regulated kinase (ERK) signal responsive repressor, Ets-2 repressive factor (ERF) is capable of forming condensates and that phosphorylation of ERF causes these condensates to dissolve. This provides a mechanism for how signal-dependent derepression can occur, and similar processes are likely to occur in other signaling pathways. Additionally, we document the dynamic dissolution and reformation of condensates during a single interphase in coordination with the export/import of ERF. This demonstrates an example of how nuclear condensates can function.

Author contributions: S.Y.S., M.S.L., and N.T. designed research; C.J.W. and N.T. performed research; C.J.W., A.L.P., and N.T. analyzed data; and C.J.W., A.L.P., S.Y.S., M.S.L., and N.T. wrote the paper.

Reviewers: S.F., Kochi Daigaku; and A.S., Georgia Institute of Technology.

The authors declare no competing interest.

[1]Present address: Department of Developmental Biology, Stanford Medicine, Stanford, CA 94305.

[2]To whom correspondence may be addressed. Email: msl2@princeton.edu or ntreen@princeton.edu.

This article contains supporting information online at http://www.pnas.org/lookup/suppl/doi:10.1073/pnas.2119187119/-/DCSupplemental.

Published February 25, 2022.

the *Ciona* embryo (*Erf.b*/*KY.Chr4.757*), while the other does not produce detectable transcripts until late larval stages (*Erf.a*/*KY.Chr4.415*). We focused our efforts on the maternal ortholog, hereafter called ERF.

Ciona ERF was fused to mNeongreen (mNg) and expressed in the embryonic ectoderm of gastrulating *Ciona* embryos using a *Sox1/2/3* regulatory sequence (Fig. 1*A*). Nuclear, punctate fluorescence is readily detected. Superresolution confocal microscopy revealed punctate distributions of ERF evocative of Hes.a repression condensates (Fig. 1*D* and *SI Appendix*, Fig. S1*A*). The corepressor for ERF has not been definitively identified, although there is evidence for potential interactions between human ERF and TLE5 (25). We observed colocalization of Gro within ERF puncta (Fig. 1*D*), suggesting that Gro functions as a corepressor of ERF in the *Ciona* embryo.

Unlike Hes.a condensates, ERF was erratically distributed across the different nuclei of individual embryos (Fig. 1*A*), which may be due to localized FGF signaling during embryonic development. To explore this possibility, ERK was activated throughout the ectoderm using a variant of human MEK

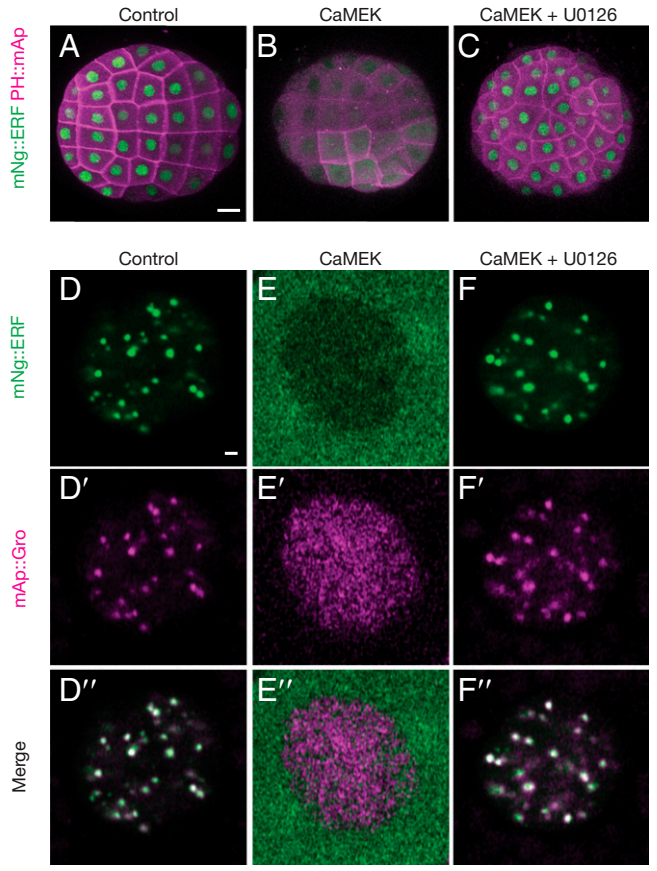

Fig. 1. ERF nuclear export is dependent on ERK phosphorylation. All panels show ectodermal cells of 110-cell stage embryos expressing electroporated transgenes of fluorescent fusion proteins. (*A*–*C*) Whole embryo views of live *Ciona* embryos with the indicated experimental treatments. Cell outlines are visualized using PH::mAp. (*A*) mNg::ERF is localized to the nucleus. Levels of nuclear fluorescence are variable between nuclei. (*B*) CaMEK overexpression causes ERF to localize outside the nucleus. (*C*) Treatment of CaMEK overexpressed embryos with the MEK inhibitor U0126 reverses the action of CaMEK, and nuclear localization of ERF is restored. (*D*–*F*) Confocal sections of single *Ciona* nuclei. (*D*, *D*′, *D*″) mNg::ERF is localized to spherical puncta that colocalize with mAp::Gro. (*E*, *E*′, *E*″) mNg::ERF is exported from the nucleus, but mAp::Gro remains nuclear when CaMEK is overexpressed. (*F*, *F*′, *F*″) This action is reversed when treated with the MEK inhibitor U0126. (Scale bars: *A*, 20 μm; *D*, 1 μm.) Fluorescent protein abbreviations: mNg mNeongreen; mAp, mApple.

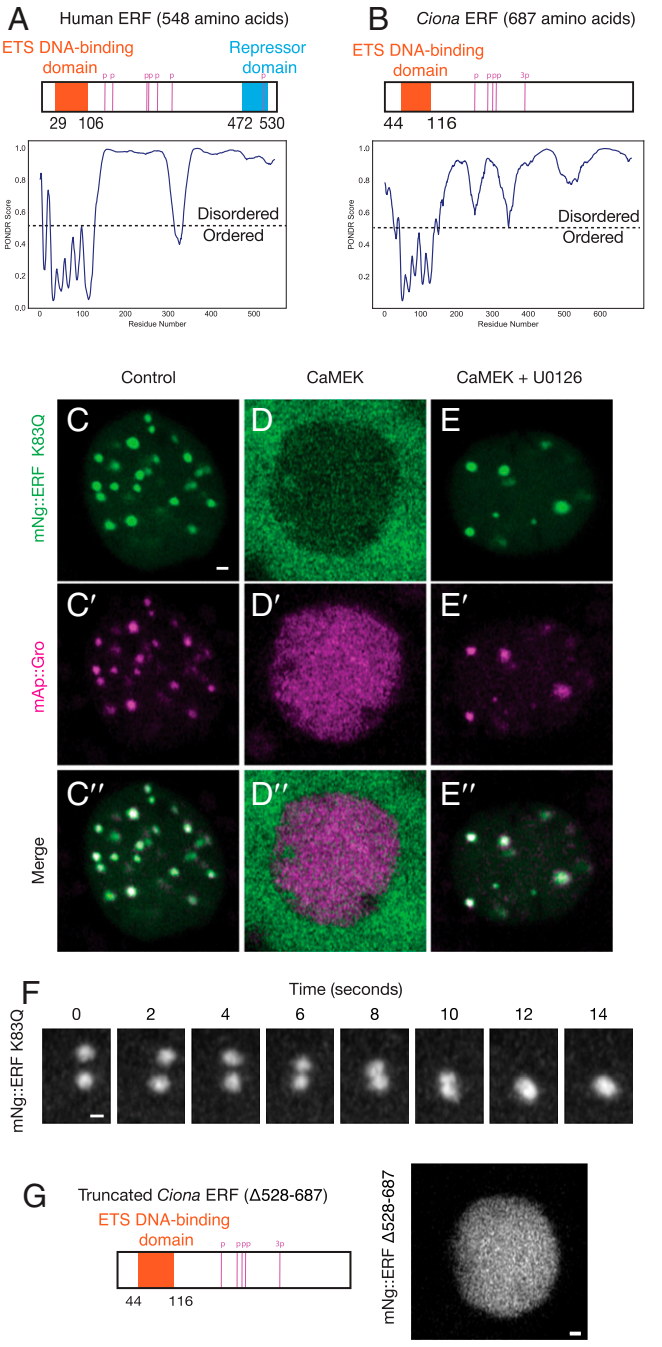

Fig. 2. ERF DNA-binding domain mutants show liquid properties. (*A* and *B*) Primary structures of human and *Ciona* ERF showing the ETS DNA-binding domain in orange and the repressor domain in blue. Potential ERK phosphorylation sites are shown in pink (p and 3p indicates 1 or 3 overlapping potential ERK phosphorylation sites). Below the structures are Predictor of Natural Disordered Regions (PONDR) plots showing the predicted ordered and disordered regions. (*C*–*E*) Confocal sections of single *Ciona* nuclei. (*C*, *C*′, *C*″) mNg::ERF K83Q is localized to spherical puncta that colocalize with mAp::Gro. (*D*, *D*, *D*″) mNg::ERF K83Q is exported from the nucleus, but mAp::Gro remains nuclear when CaMEK is overexpressed. (*E*, *E*′, *E*″) This action is reversed when treated with the MEK inhibitor U0126. (*F*) Maximum-intensity confocal projection showing the fusion of 2 mNg::ERF K83Q droplets over 14 s. (*G*) Structure of *Ciona* ERF where 160 residues were deleted from the C terminus (Δ528-687) and a confocal section of a single nucleus expressing mNg::ERF Δ528-687. (Scale bars: *C* and *G*, 1 μm; *F*, 0.5 μm.) Fluorescent protein abbreviations: mNg mNeongreen; mAp, mApple.

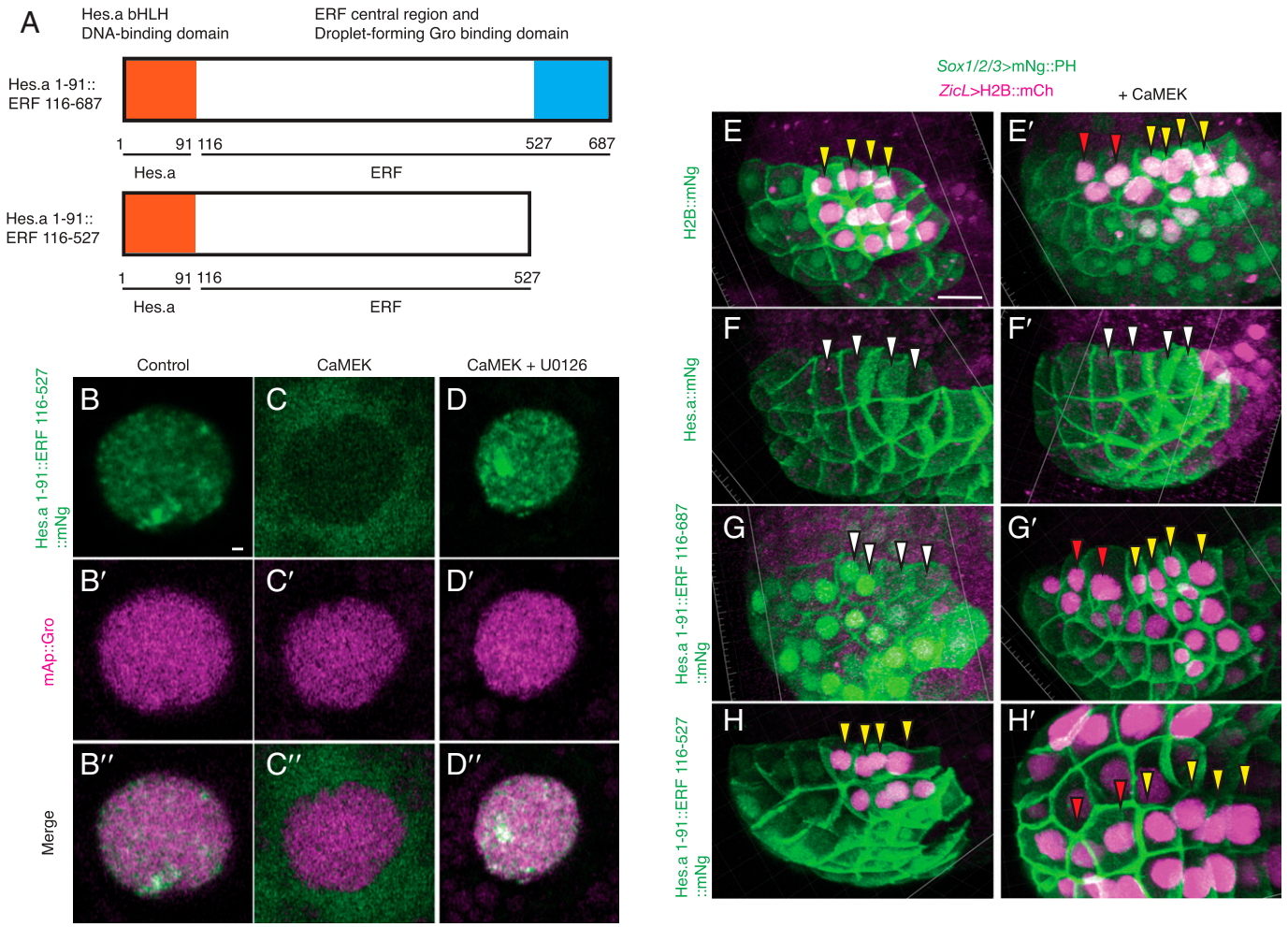

Fig. 3. *Ciona* ERF contains a C-terminal repressor domain. (*A*) Primary structures of Hes.a/ERF chimera proteins with the DNA-binding and droplet-forming domains indicated. (*B–D*) Confocal sections of single *Ciona* nuclei. Hes.a 1-91::ERF 116-527::mNg is localized to puncta that do not colocalize with mAp::Gro. Hes.a 1-91::ERF 116-527::mNg is exported from the nucleus, but mAp::Gro remains nuclear when CaMEK is overexpressed. This action is reversed when treated with the MEK inhibitor U0126. (*E* and *E′*) Expression of ZicL reporter in the *Ciona* neural plate is expanded anteriorly when CaMEK is expressed. (*F* and *F′*) Hes.a::mNg represses all ZicL expression in the neural plate. (*G* and *G′*) Hes.a 1-91::ERF 116-687::mNG represses ZicL. This repression is inactivated by CaMEK. (*H* and *H′*) Hes.a 1-91::ERF 116-527::mNg is unable to repress ZicL. Yellow arrowheads indicate wild-type expression. Red arrowheads indicate ectopic expression. White arrowheads indicate repression of wild-type expression. Cell outlines are indicated with PH::mNg as in several cases the transcription factors of interest are degraded by the time reporter activity is detectable. (Scale bars: *B*, 1 μm; *E*, 10 μm.) Fluorescent protein abbreviations:mNg mNeongreen; mAp, mApple; mCh, mCherry.

(CaMEK) that possesses greater constitutive activity than commonly used phosphomimetic variants (26). This experimental activation of MEK caused ERF to be excluded from all nuclei (Fig. 1*B*) and demonstrates ERF localization is dependent on ERK signaling. When treated with the MEK inhibitor U0126, ERF nuclear exclusion is reversed, and nuclear accumulation is restored (Fig. 1*C*).

Coexpression of CaMEK not only led to export of ERF from the nucleus but also caused a loss of ERF puncta (Fig. 1*E*). This observation is similar to when the WRPW domain was removed from Hes.a (9), Gro puncta were also lost, suggesting that these overexpression experiments may exaggerate the size of repressive condensates at these early developmental stages. These puncta are restored upon addition of the U0126 inhibitor (Fig. 1*F*), suggesting that ERF/Gro complexes are specific targets of ERK signaling. By contrast, activation or inhibition of ERK had no noticeable effect on Hes.a condensates (*SI Appendix*, Fig. S1).

Human ERF has an N-terminal ETS DNA-binding domain followed by a disordered domain. A region of this disordered sequence (residues 472–530) is essential for repression (Fig. 2*A*) (15). The *Ciona* homolog of ERF has a similar N-terminal ETS domain, but also contains an additional 139 amino acid (AA) residues in the C terminus (Fig. 2*B*; see below). This region is less disordered than its human counterpart (Fig. 2*B*). It was previously shown that mutations in the DNA-binding domain of Hes.a resulted in condensates exhibiting definitive liquid-like properties (9). We similarly observed that a K83Q mutation in the ERF ETS DNA-binding domain forms fewer, larger puncta that retain association with Gro (Fig. 2*C*). This mutation mimics a human clinical variant associated with craniosynostosis (24). The mutant condensates display similar responses to activated or inhibited MEK as their wild-type counterparts (Fig. 2 *D* and *E*), suggesting that responses to ERK signaling can occur irrespective of DNA binding. They also exhibit fusions of individual puncta, consistent with the formation of ERF/Gro repression condensates via LLPS (Fig. 2*F* and Movie S1).

To identify a putative repression domain, we created a series of truncations of ERF. Removal of the C-terminal 140 AA residues disrupted droplet formation, while loss of an additional 20 AA residues resulted in uniform distribution throughout the nucleus (Fig. 2*G* and *SI Appendix*, Fig. S2*A*). This behavior is

similar to previous observations of Hes.a where the removal of the Gro-interaction motif (WRPW) abolished droplet formation (9). Based on these observations, we designate the C-terminal 160 residues of *Ciona* ERF as a droplet-forming domain (*SI Appendix*, Fig. S2*B*).

We next asked whether this domain mediates repression. Previous studies showed that chimeric proteins replacing the DNA-binding domain of human ERF with the DNA-binding domains of other transcription factors were found to retain ERK-modulated repression activities (15). We therefore replaced the ETS DNA-binding domain of *Ciona* ERF with the bHLH DNA-binding domain of Hes.a (Fig. 3*A*). The resulting chimera forms nuclear puncta (*SI Appendix*, Fig. S3*A*), displays colocalization with Gro, and is imported and exported from nuclei in response to experimental manipulation of MEK (*SI Appendix*, Fig. S3 *B* and *C*). Removal of the 160 AA droplet-forming domain from this chimeric protein resulted in a loss of droplets and Gro colocalization (Fig. 3 *B–D*).

The Hes.a/ERF chimera appears to repress a Hes.a target gene in response to FGF/ERK signaling. The Hes.a target gene ZicL (27) is expressed in neuronal precursor cells of rows I to IV of the presumptive neural plate (28). A reporter containing the upstream regulatory sequences of *ZicL* recapitulates this localized pattern of expression (Fig. 3*E*) (20). Coexpression of CaMEK throughout the early ectoderm results in an anterior expansion of the *ZicL* reporter gene (Fig. 3*E′*). Hes.a has previously been shown to repress this reporter (Fig. 3*F*) (9), and it continues to do so even upon coexpression of CaMEK (Fig. 3*F′*). By contrast, the Hes.a/ERF chimera represses *ZicL* in the neural plate, but weak expression of the *ZicL* reporter as well as a loss of nuclear Hes.a/ERF could be seen in posterior cells that are adjacent to a localized source of FGF/ERK signaling (Fig. 3*G*) (29). Moreover, repression is completely abolished when CaMEK is expressed throughout the neural plate when the C-terminal droplet-forming, Gro-binding domain of ERF is deleted (Fig. 3 *G′–H′*). These observations suggest that the C-terminal 160 residues of the ERF protein are required for repression by recruiting Gro and are modulated by FGF/ERK signaling (Fig. 3 *H* and *H′*).

Live imaging of gastrulating embryos revealed dynamic import and export of ERF from the nucleus over the course of a single interphase (Fig. 4*A* and *SI Appendix*, Fig. S4 and Movies S2 and S3). This behavior was variable, both within a single embryo and between replicates, with some cells having

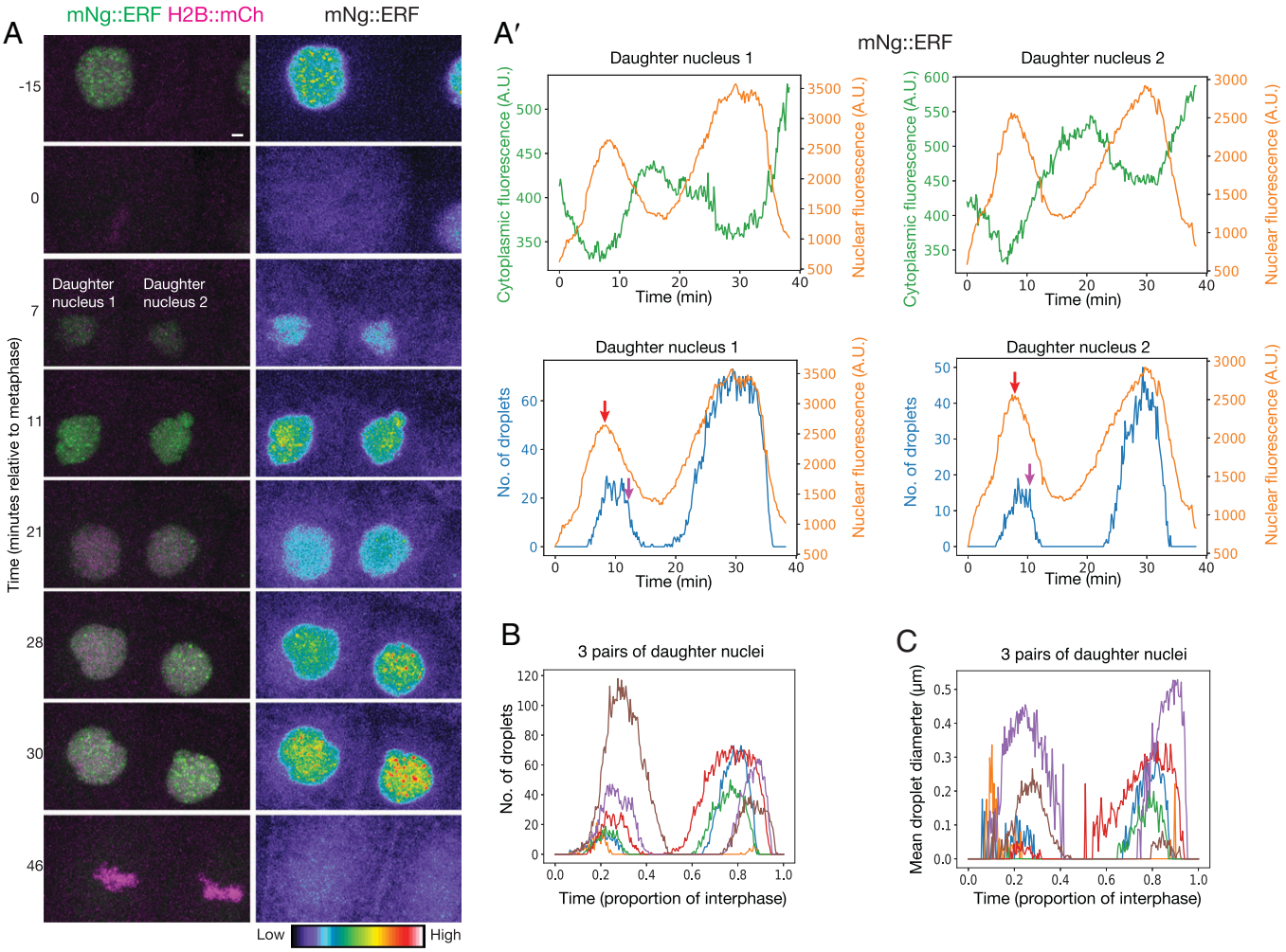

Fig. 4. ERF pulses during interphase. (*A*) Maximum intensity confocal projection of a *Ciona* nucleus dividing and the daughter nuclei throughout interphase. mNg::ERF is exported from and to imported from the nucleus throughout interphase. (Scale bar: 1 µm.) (*A′*) Quantifications of the nuclear fluorescence intensity, number of droplets, and cytoplasmic fluorescence intensity of the daughter nuclei in *A*. Red arrows indicate the approximate time that nuclear fluorescence intensity decreases, and pink arrows indicate the approximate time that number of droplets abruptly decreases. (*B* and *C*) Quantifications of number of mNg::ERF droplets and the mean diameter of droplets from the six nuclei in *A* and *SI Appendix*, Fig. S4*B*. Time is normalized to the relative proportion of interphase. A.U.: arbitrary units. Fluorescent protein abbreviations: mNg mNeongreen; mCh, mCherry.

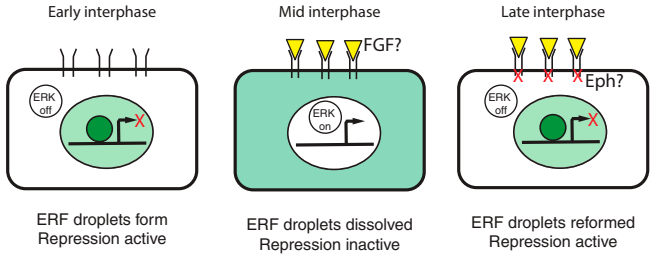

Fig. 5. ERF derepression by dissolution of repressive condensates. At early interphase, in the absence of an inductive signal, ERK is inactive, and ERF is localized to the nucleus, where it forms repressive condensates as well as a dilute phase. When a signal is present (yellow arrowheads, for example, FGF), activated ERK enters the nucleus and will immediately phosphorylate ERF, causing it to be exported from the nucleus and repressive condensates to dissolve. After an extended or intense period of signaling, the repressive condensates will dissolve, and transcriptional activation can proceed. After several minutes, the signal can be attenuated (possibly by Eph/Ephrin). After signal attenuation, ERF can reenter the nucleus and phase separate to form repressive condensates reinstating repression.

ERF remain nuclear while others displayed complete exclusion from the nucleus throughout interphase (Movies S2 and S3). This variability may be due to receipt of localized FGF signals by specific cells (see *Discussion*).

ERF condensates were limited to ~500 nm in diameter even upon complete inhibition of ERK signaling with U0126 (*SI Appendix*, Fig. S5 *A–C* and Movies S4 and S5). Consistent with previously observed Hes.a condensate behaviors (9), the DNA-binding domain mutant formed fewer and larger droplets (*SI Appendix*, Fig. S5 *D–F* and Movie S4). Pulsatile behavior was still observed, although the initial formation of condensates was short-lived (*SI Appendix*, Fig. S5 *D* and *E* and Movies S6 and S7). When treated with U0126, mutant ERF condensates continued to grow and fuse to sizes over 1 μm, considerably larger than wild-type condensates (*SI Appendix*, Fig. S5 *G–I* and Movies S8 and S9). These observations suggest that ERF condensate growth is limited by both DNA binding and ERK phosphorylation. Pulsatile behavior was never observed when embryos were treated with U0126 (*SI Appendix*, Fig. S5 *D*, *E*, and *G–I*), suggesting that nuclear export and dissolution is due to ERK signaling.

We observed that nuclear export is accompanied by a decrease in nuclear fluorescence and a concurrent increase in cytoplasmic fluorescence (Fig. 4*A*′). While nuclear fluorescence decreases, droplet number remains relatively unchanged for 3 to 5 min. After this lag, there is a sudden and uniform dissolution of ERF/Gro condensates (Fig. 4 *A* and *B* and *SI Appendix*, Fig. S4), suggesting ERK-mediated export precedes dissolution. This behavior is not observed at mitosis, where the decrease in nuclear florescence and dissolution of droplets were tightly correlated (Fig. 4 and *SI Appendix*, Fig. S4). We discuss the implications of these observations below.

Discussion

We have presented evidence that ERF associates with Gro and forms repression condensates. This association depends on an extended C-terminal region that is required for the recruitment of Gro, the formation of condensates, and transcriptional repression. This differs from the short, dedicated WRPW motif that mediates Hes.a-Gro associations, raising the possibility of distinct modes of condensate formation for Hes.a and ERF. A particularly striking finding of our analysis is the pulsatile assembly and dissolution of ERF/Gro condensates during interphase. These dynamics sharply contrast with the assembly of stable Hes.a condensates, highlighting the role of FGF/ERK signaling in the precision of gene activity.

ERK signaling pathways often display oscillatory or pulsatile dynamics (30, 31). However, this behavior was not anticipated for early *Ciona* embryos since all signaling events, including FGF signaling, are characterized by stable direct cell–cell contacts (18, 32, 33). Nonetheless, we observe clear pulses of ERF/Gro assembly and disassembly during interphase. These observations suggest pulsing cells have a short permissive period for response to ERK signaling during the cell cycle, despite sustained cell–cell contacts. This restrictive period of response might suppress noise and help ensure switch-like induction of gene activity by extracellular signals such as FGF.

Previous studies have implicated Ephrin as a key antagonist of FGF signaling in *Ciona* (34, 35), raising the possibility that Ephrin inhibition works in concert with LLPS to ensure transcriptional precision. It was recently shown that knockdown of ERF causes ectopic expression of Otx at the 32-cell stage (36). It is likely that ERF modulates OTX expression along with the geometry of cell–cell contacts, the levels of RTK receptors and ligands, as well as the action of the Eph/Ephrin antagonist. We note, however, that Ephrin activities are mainly detected at earlier or later stages of development than those examined in this study. Future studies will explore the relative roles of LLPS and Ephrin in the control of gene activity by FGF and other mediators of ERK signaling.

How does ERK signaling trigger the dissociation of ERF/Gro condensates? We tested the possibility that it might be due to ERF nuclear export. The idea is that export would trigger a domino effect, whereby ERF in the condensed phase would be released to compensate for reduced concentrations of ERF in the dilute phase. To test this idea, we treated embryos with leptomycin B, a drug shown to inhibit export of mammalian ERF (23). ERF/Gro condensates appear to dissolve on schedule despite this block in ERF nuclear export (*SI Appendix*, Fig. S6). These observations are consistent with fast derepression of genes in the *Drosophila* embryo, which occurs before ERK signals lead to nuclear export of the Capicua repressor (13, 37).

We therefore suggest that ERK-mediated phosphorylation underlies the dissolution of ERF repression condensates (Fig. 5). However, this remains speculative, and it is currently uncertain whether phosphorylation occurs in the dilute phase, the condensed phase, or both. Regardless of mechanism, the dissolution of repression condensates is an inherently effective mechanism for the rapid, switch-like induction of gene expression in response to cell–cell signaling. It seems likely that a similar strategy is used for a variety of developmental patterning processes.

Methods

Animals. Wild *Ciona intestinalis* (Pacific populations, type A, also referred to as *Ciona robusta*) adults were commercially sourced from San Diego County, CA, by M-Rep. Animals were kept in aerated artificial seawater at 18 °C. U0126 treatment concentration was 8 μM. Leptomycin B treatment concentration was 0.2 μM. Control embryos were treated with either 0.1% dimethyl sulfoxide or ethanol.

Molecular Cloning. All novel plasmids constructed for this study were based on the *pSP Sox1/2/3>* plasmid previously described (9) with the open reading frames replaced by PCR amplifications using a proofreading DNA polymerase (Primestar, Takara), and plasmids were assembled from linear PCR products using the NEBuilder HiFi DNA Assembly Master Mix (New England Biolabs). Fluorescent moieties of fusion proteins were separated by the linker sequence GGSGGGSGG. Full gene names, synonyms, and primers used to amplify complementary DNA sequences are listed in *SI Appendix*, Table S1. Truncations and modifications of Hes.a and ERF were based on the longest open reading frames of the predicted transcripts *KH.C1.159.v1.R.nonSL2-1* (*Hes.a*) and *KH.C4.366.v1.A.ND1-1* (*ERF*). Full plasmid sequences and descriptions of the individual cloning steps can be provided upon request. The *ZicL > H2B::mCherry* plasmid has previously been described (29). The constitutively active variant of human MEK has been previously described (26).

Electroporations. Dechorionated *Ciona* zygotes were electroporated as previously described (9). Electroporations were performed in 800-μL volumes containing 0.54 M mannitol, 230-μL artificial sea water, and approximately 300 *Ciona* zygotes. For each plasmid, 40 μg was electroporated for all conditions except *Sox1/2/3 > PH::mApple* and *ZicL > H2B::mCherry*, where 60 μg and 20 μg, respectively was electroporated. All experiments were replicated at least in triplicate using different batches of *Ciona* eggs.

Imaging. Imaging was performed as previously described (9) using a Zeiss 880 confocal microscope equipped with an Airyscan detector in fast mode. Exact settings and raw imaging files are available upon request.

Image Analysis. All images were Airyscan-processed using Zeiss Zen software (ZEN Version 2.3 and 2.6, Zeiss) The identification and quantification of droplets from confocal images were performed using the *Imaris* spot detection function. All conditions were quantified using the green fluorescence channel across all conditions. Estimated sizes of droplets ranged from 0.2 to 0.3 μm (wild type and mutant ERF) and 0.5 μm (inhibitor treatments). Background subtraction and region growing were accounted for throughout the cell cycle to accurately report droplet quantity and size. Droplet number in Imaris was filtered using the quality filter, setting a droplet threshold of 95% to prevent false droplet identification. The absolute intensity was used to determine spot regions/diameters. All statistics were exported from Imaris. Further processing was done in Python to fill in the information for frames without droplets as containing 0 droplets of diameter 0. All values exactly equal to the cutoff were excluded from further analysis. The remaining values were normalized to cell cycle length and plotted using matplotlib.

Nuclear and cytoplasmic fluorescence quantification of mNg::ERF was performed in Fiji. A nuclear and cytoplasmic mask was defined, and average fluorescence intensities were recorded. Data were plotted alongside droplet data using matplotlib.

Data Availability. All data are included in the manuscript and/or supporting information.

ACKNOWLEDGMENTS. We thank Clifford Brangwynne, Ned Wingreen, and members of the Levine and Brangwynne laboratories for helpful discussions. We thank Chris Killen for video editing. This research was funded by an NIH grant (NS076542) to M.S.L. N.T. is funded by a Princeton Catalysis Initiative grant. C.J.W. is funded by a NSF graduate research fellowship.

1. A. A. Hyman, C. A. Weber, F. Jülicher, Liquid–liquid phase separation in biology. *Annu. Rev. Cell Dev. Biol.* **30**, 39–58 (2014).
2. A. R. Strom, C. P. Brangwynne, The liquid nucleome — Phase transitions in the nucleus at a glance. *J. Cell Sci.* **132**, 1–7 (2019).
3. C. P. Brangwynne, T. J. Mitchison, A. A. Hyman, Active liquid-like behavior of nucleoli determines their size and shape in *Xenopus laevis* oocytes. *Proc. Natl. Acad. Sci. U.S.A.* **108**, 4334–4339 (2011).
4. W. K. Cho *et al.*, Mediator and RNA polymerase II clusters associate in transcription-dependent condensates. *Science* **361**, 412–415 (2018).
5. B. R. Sabari *et al.*, Coactivator condensation at super-enhancers links phase separation and gene control. *Science* **361**, eaar3958 (2018).
6. A. Boija *et al.*, Transcription factors activate genes through the phase-separation capacity of their activation domains. *Cell* **175**, 1842–1855.e16 (2018).
7. A. G. Larson *et al.*, Liquid droplet formation by HP1α suggests a role for phase separation in heterochromatin. *Nature* **547**, 236–240 (2017).
8. A. R. Strom *et al.*, Phase separation drives heterochromatin domain formation. *Nature* **547**, 241–245 (2017).
9. N. Treen, S. F. Shimobayashi, J. Eeftens, C. P. Brangwynne, M. Levine, Properties of repression condensates in living Ciona embryos. *Nat. Commun.* **12**, 1561 (2021).
10. S. Barolo, J. W. Posakony, Three habits of highly effective signaling pathways: Principles of transcriptional control by developmental cell signaling. *Genes Dev.* **16**, 1167–1181 (2002).
11. M. Affolter, G. Pyrowolakis, A. Weiss, K. Basler, Signal-induced repression: The exception or the rule in developmental signaling? *Dev. Cell* **15**, 11–22 (2008).
12. A. L. Patel, S. Y. Shvartsman, Outstanding questions in developmental ERK signaling. *Development* **145**, dev143818 (2018).
13. G. Jiménez, S. Y. Shvartsman, Z. Paroush, The Capicua repressor—A general sensor of RTK signaling in development and disease. *J. Cell Sci.* **125**, 1383–1391 (2012).
14. E. M. O'Neill, I. Rebay, R. Tjian, G. M. Rubin, The activities of two Ets-related transcription factors required for *Drosophila* eye development are modulated by the Ras/MAPK pathway. *Cell* **78**, 137–147 (1994).
15. D. N. Sgouras *et al.*, ERF: An ETS domain protein with strong transcriptional repressor activity, can suppress ets-associated tumorigenesis and is regulated by phosphorylation during cell cycle and mitogenic stimulation. *EMBO J.* **14**, 4781–4793 (1995).
16. G. Mavrothalassitis, J. Ghysdael, Proteins of the ETS family with transcriptional repressor activity. *Oncogene* **19**, 6524–6532 (2000).
17. A. D. Sharrocks, The ETS-domain transcription factor family. *Nat. Rev. Mol. Cell Biol.* **2**, 827–837 (2001).
18. P. Lemaire, Unfolding a chordate developmental program, one cell at a time: Invariant cell lineages, short-range inductions and evolutionary plasticity in ascidians. *Dev. Biol.* **332**, 48–60 (2009).
19. B. Davidson, W. Shi, J. Beh, L. Christiaen, M. Levine, FGF signaling delineates the cardiac progenitor field in the simple chordate, Ciona intestinalis. *Genes Dev.* **20**, 2728–2738 (2006).
20. T. B. Gainous, E. Wagner, M. Levine, Diverse ETS transcription factors mediate FGF signaling in the Ciona anterior neural plate. *Dev. Biol.* **399**, 218–225 (2015).
21. K. S. Imai, K. Hino, K. Yagi, N. Satoh, Y. Satou, Gene expression profiles of transcription factors and signaling molecules in the ascidian embryo: Towards a comprehensive understanding of gene networks. *Development* **131**, 4047–4058 (2004).
22. D. Liu, E. Pavlopoulos, W. Modi, N. Moschonas, G. Mavrothalassitis, ERF: Genomic organization, chromosomal localization and promoter analysis of the human and mouse genes. *Oncogene* **14**, 1445–1451 (1997).
23. L. Le Gallic, D. Sgouras, G. Beal Jr., G. Mavrothalassitis, Transcriptional repressor ERF is a Ras/mitogen-activated protein kinase target that regulates cellular proliferation. *Mol. Cell. Biol.* **19**, 4121–4133 (1999).
24. S. R. F. Twigg *et al.*, Reduced dosage of ERF causes complex craniosynostosis in humans and mice and links ERK1/2 signaling to regulation of osteogenesis. *Nat. Genet.* **45**, 308–313 (2013).
25. K. Luck *et al.*, A reference map of the human binary protein interactome. *Nature* **580**, 402–408 (2020).
26. Y. Goyal *et al.*, Divergent effects of intrinsically active MEK variants on developmental Ras signaling. *Nat. Genet.* **49**, 465–469 (2017).
27. T. Ikeda, T. Matsuoka, Y. Satou, A time delay gene circuit is required for palp formation in the ascidian embryo. *Development* **140**, 4703–4708 (2013).
28. K. S. Imai, M. Levine, N. Satoh, Y. Satou, Regulatory blueprint for a chordate embryo. *Science* **312**, 1183–1187 (2006).
29. E. Wagner, M. Levine, FGF signaling establishes the anterior border of the Ciona neural tube. *Development* **139**, 2351–2359 (2012).
30. A. G. Goglia *et al.*, A live-cell screen for altered Erk dynamics reveals principles of proliferative control. *Cell Syst.* **10**, 240–253.e6 (2020).
31. T. Hiratsuka *et al.*, Intercellular propagation of extracellular signal-regulated kinase activation revealed by in vivo imaging of mouse skin. *eLife* **4**, e05178 (2015).
32. N. Ohta, Y. Satou, Multiple signaling pathways coordinate to induce a threshold response in a chordate embryo. *PLoS Genet.* **9**, e1003818 (2013).
33. L. Guignard *et al.*, Contact area-dependent cell communication and the morphological invariance of ascidian embryogenesis. *Science* **369**, eaar5663 (2020).
34. W. Shi, M. Levine, Ephrin signaling establishes asymmetric cell fates in an endomesoderm lineage of the Ciona embryo. *Development* **135**, 931–940 (2008).
35. N. Haupaix *et al.*, Ephrin-mediated restriction of ERK1/2 activity delimits the number of pigment cells in the Ciona CNS. *Dev. Biol.* **394**, 170–180 (2014).
36. G. Williaume *et al.*, Cell geometry, signal dampening, and a bimodal transcriptional response underlie the spatial precision of an ERK-mediated embryonic induction. *Dev. Cell* **56**, 2966–2979.e10 (2021).
37. S. E. Keenan *et al.*, Rapid dynamics of signal-dependent transcriptional repression by capicua. *Dev. Cell* **52**, 794–801.e4 (2020).